

Self-sustained oscillations in nanoelectromechanical systems induced by Kondo resonance

Taegeun Song¹, Mikhail N Kiselev¹, Konstantin Kikoin^{1,2},
Robert I Shekhter³ and Leonid Y Gorelik⁴

¹The Abdus Salam International Center for Theoretical Physics, Strada Costiera 11, I-34151 Trieste, Italy

²School of Physics and Astronomy, Tel-Aviv University, Tel-Aviv 69978, Israel

³Department of Physics, University of Gothenburg, SE-412 96 Göteborg, Sweden

⁴Department of Applied Physics, Chalmers University of Technology, SE-412 96 Göteborg, Sweden

E-mail: tsong@ictp.it

Received 29 November 2013

Accepted for publication 21 February 2014

Published 31 March 2014

New Journal of Physics **16** (2014) 033043

[doi:10.1088/1367-2630/16/3/033043](https://doi.org/10.1088/1367-2630/16/3/033043)

Abstract

We investigate the instability and dynamical properties of nanoelectromechanical systems represented by a single-electron device containing movable quantum dots attached to a vibrating cantilever via asymmetric tunnel contacts. The Kondo resonance in electron tunneling between the source and shuttle facilitates self-sustained oscillations originating from the strong coupling of mechanical and electronic/spin degrees of freedom. We analyze a stability diagram for the two-channel Kondo shuttling regime due to limitations given by the electromotive force acting on a moving shuttle, and find that the saturation oscillation amplitude is associated with the retardation effect of the Kondo cloud. The results shed light on possible ways to experimentally realize the Kondo-cloud dynamical probe by using high mechanical dissipation tunability as well as supersensitive detection of mechanical displacement.

Keywords: nanomechanics, resonance scattering, self-sustained oscillations



Content from this work may be used under the terms of the [Creative Commons Attribution 3.0 licence](https://creativecommons.org/licenses/by/3.0/).

Any further distribution of this work must maintain attribution to the author(s) and the title of the work, journal citation and DOI.

1. Introduction

Recent progress in nanotechnology has made it possible to fabricate nanodevices in which the mechanical degrees of freedom are strongly coupled not only to the electronic charge (nanoelectromechanics (NEM)), but also the spin degrees of freedom (nanospinromechanics (NSM)) [1, 2]. While manipulating the charge degrees of freedom requires the energies/external voltages determined by the Coulomb interaction in the nanodevice (the charging energy of the quantum dots), spin manipulation needs much smaller scales of the energy determined by exchange interaction. Therefore, on the one hand, spin manipulation is free of heating problems, and on the other, it allows one to achieve very high device efficiency [3].

A special case where the spin degrees of freedom are dominant in quantum transport is the Kondo effect, which manifests itself as a resonance scattering of electrons on the impurity spin [4, 5]. The retardation effects in NEM devices result in two-channel Kondo tunneling, which enhances both spin and charge transport due to maximal overlap of the wave functions of the electrons in the leads [2, 3]. These processes are mediated by the spin flip of the localized state in the dot. Another facet of the Kondo effect is the formation of a screening cloud of conduction electrons, which ‘dresses’ the quantum impurity spin. The typical length scale of the screening cloud is $\sim 1\mu\text{m}$ [6]. There have been several proposals to detect the size of the Kondo however, unambiguous results are still not available and there has been no conclusive measurement due to quantum fluctuations with zero-averaged spin [14].

We are interested in the new effects where a moving quantum impurity is nano-machined by attaching it to a nano-mechanical device. Such devices are realized as quantum dots incorporated into a mechanical system that oscillates between two metallic leads. These mechanical systems include long cantilever nanorelay [15], atomic force microscopy with a tip [16, 17] and a nanoisland attached either to the cantilever [18] or to one of the leads [16, 17]. A basic understanding of the NEM/NSM has been achieved in both theoretical [19–25] and experimental [26, 27] studies of single-electron shuttling. Alternatively, the mechanical system can itself play the role of one of the contacts when the quantum dot (impurity) is deposited on top of the metallic cantilever [18]. In these cases, either one or two tunnel barriers change shape in the mechanical motion process, thus providing a coupling of the mechanical and electronic/spin degrees of freedom.

The temporal dynamics of the Kondo cloud are governed by two main effects. First, the cloud adiabatically follows a position of quantum impurity, and second, the size of the cloud changes in time due to the change in tunnel matrix elements. Both these effects are accompanied by retardation processes similar to those that determine the polaronic effects due to strong electron–phonon interaction. But how do the dynamics of the Kondo cloud affect the mechanical system, and how can one probe these dynamics? Is it possible to control the cloud’s size? Some of these questions have been addressed in a recent publication [3]. This study showed that the mechanical dissipation is controlled by the kinetics of Kondo screening if an electric dc current is transmitted through the system in the presence of an external magnetic field. Besides, the characteristic time determining the kinetics of Kondo screening may be measured through the mechanical quality factor. Thus, the strong coupling of the spin with the mechanical subsystem allows a superhigh tunability of mechanical dissipation as well as supersensitive detection of the mechanical displacement.

In this paper, we address the question of whether such a strong coupling between the mechanics and spintronics can drive the system from an almost adiabatic regime of small

amplitude mechanical vibrations to a steady-state regime with large-amplitude self-sustained oscillations. As an example of such a regime, we consider an instability associated with the appearance of self-sustained oscillations in the system induced by ‘Kondo friction’. It will be shown that this regime can be controlled by electric (source–drain voltage, gate voltage) and magnetic fields. We analyse the sensitivity of solutions to the initial conditions and construct a complete phase diagram of the model. We show that the system possesses reach non-linear dynamics (Hopf-pitchfork bifurcation), and demonstrate that by controlling the displacements (velocities) of the mechanical system with a high precision, one can manipulate both the spin and charge tunnel currents.

2. Model

A sketch of the system under consideration is presented in figure 1 (a). A nano-island is mounted on the metallic cantilever attached to the drain electrode. The distance between the source electrode and the island, and thus the tunnel coupling between them, depends on the cantilever motion. An external magnetic field is applied perpendicularly to the cantilever far from the island. In our consideration, the flexural vibration of the nanowire is restricted to the dynamics of the fundamental mode only. This is treated as a damped harmonic oscillator with frequency ω_0 , and quality factor Q_0 .

The equation of mechanical motion for the Kondo-NEM coupling device is given by:

$$\ddot{u} + \frac{\omega_0}{Q_0}\dot{u} + \omega_0^2 u = \frac{1}{m} [(L \cdot I \cdot B) + F_K] \quad (1)$$

where u describes the cantilever’s displacement of the free end (see figure 1(a)) and m is the effective mass. The right-hand-side of equation (1) includes the Lorentz force acting on a metallic cantilever in the presence of the effective magnetic field B and the ‘Kondo force’ associated with the coordinate dependence of the ground-state Kondo energy $E_{gs} \sim T_K(u)$ [28]⁵. Here, L is the cantilever length and the I current through the cantilever equals $I = I_{dc} + I_{ac} + I_{emf}$. Two of the first terms contributing to the tunnel current have been calculated in the adiabatic approximation in the limit of strong Kondo coupling at $T \ll T_K$, where the Kondo temperature T_K depends parametrically on time via cantilever vibration in a reasonable assumption that the mechanical motion of a shuttle is slow in comparison with all the characteristic times for Kondo tunneling [3]: I_{dc} corresponds to a time-modulated dc component, I_{ac} is an ac component associated with the modulation of the Kondo cloud located deeply inside the leads

$$I_{dc} = 2G_0 V_{bias} \cosh^{-2} \left[\frac{u(t) - u_0}{\lambda} \right] \quad (2)$$

⁵ The Kondo force accounts for a universal (cutoff independent) contribution to the ground state energy. However, there also exists a non-universal (cutoff dependent) part of the ground state energy, see, e.g., [29]. We assume that this part is absorbed into the definition of ω_0 due to the coordinate dependence of the Kondo energy.

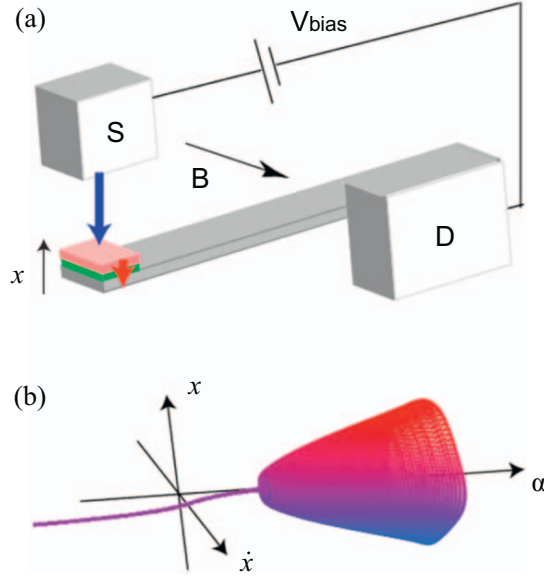


Figure 1. (a) A shuttle with a cantilever: the quantum dot (pink) is deposited on top of a metallic cantilever. The constant width tunnel barrier between the dot and metallic reservoir is depicted in green. The source–shuttle barrier changes its width when the device oscillates. The blue and red arrows indicate an asymmetry of the tunnel barrier widths. The device is subject to an external source (S), drain (D), voltage V_{bias} and external magnetic field B , applied perpendicularly to the plane of oscillations. x denotes a dimensionless displacement (in units of tunnel length) measured from the equilibrium position of the shuttle. (b) The evolution of the phase space $\{x, \dot{x}\}$ as a function of universal parameter α (dimensionless force, see below for discussion). One can see the appearance of instability at some critical value of this control parameter.

$$I_{ac} = \frac{\dot{u}(t)}{\lambda} \frac{eE_c}{8\Gamma_0} \frac{eV_{\text{bias}}}{k_B T_K(t)} \frac{\tanh\left(\frac{u(t)-u_0}{\lambda}\right)}{\cosh^2\left(\frac{u(t)-u_0}{\lambda}\right)}. \quad (3)$$

Here, $G_0 = e^2/h$ is the unitary conductance per spin projection, V_{bias} is the bias voltage, and λ is the tunneling length for the source–island tunnel barrier. The Kondo temperature for the moving island is

$$k_B T_K(t) \equiv k_B T_K[u(t)] = D_0 \exp\left[-\frac{\pi E_c}{4(\Gamma_s(u) + \Gamma_d)}\right],$$

where E_c is the charging energy of the dot, $\Gamma_d = \Gamma_0$ and $\Gamma_s(u) = \Gamma_0 \exp\{2(u - u_0)/\lambda\}$ are the island–drain (d) and island–source (s) tunnel rates, and D_0 is the effective bandwidth for the electrons in the leads. Thus, I_{ac} describes the Ohmic regime where the time dependence is associated with the $\cosh^{-2}[(u(t) - u_0)/\lambda]$ Breit–Wigner factor given by the time-dependent tunnel widths. In contrast to this, the major time dependence of I_{ac} is connected to the time modulations of the Kondo temperature $T_K(t)$.

The final contribution to the current I is $I_{emf} = -G_0 \dot{u}LB$. This term is related to the voltage difference $\mathcal{E} = -\dot{u}LB$ between the electrodes induced by the motion of the metallic cantilever in the effective magnetic field, B . As a result, the velocity dependent current term I_{ac} is modified by the factor $1 - \Delta(u)$, where $\Delta \propto (\Gamma_0/E_c)(k_B T_K/eV_{bias})(\lambda LB/\phi_0)$, $\phi_0 = h/(2e)$ is a magnetic flux quanta. Thus, the electromotive force $\sim B^2$ is immaterial in the regime of weak magnetic fields.

3. Amplitude dynamics

First, we analyse the amplitude dynamics and stability of the system without the emf term, and then consider a regime where the emf term plays an important role. It is convenient to introduce the dimensionless equation of motions using equation (1) scaled by tunnel length λ , ($x \equiv u(t)/\lambda$) and dimensionless time scaled with ω_0^{-1} :

$$\ddot{x} + \gamma \dot{x} + x = \frac{\alpha_K(t) + \alpha}{\cosh^2(x - x_0)} - \dot{x} \alpha \tau_\beta f(x - x_0), \quad (4)$$

In these notations, $\alpha = \frac{2G_0 V_{bias} BL}{m\omega_0^2 \lambda}$, $\alpha_K(t) = -\frac{\pi E_c k_B T_K(t)}{8\Gamma_0 m \omega_0^2 \lambda^2}$ are the dimensionless Lorentz and Kondo forces, respectively, $\beta = \frac{\pi E_c}{4 T_0}$ is the coupling strength of the electronic states, $\gamma = \frac{1}{Q_0}$ is the mechanical friction coefficient, and x_0 is the dimensionless parameter $x_0 = u_0/\lambda$ characterizing the asymmetry of the system at the equilibrium position such that $\Gamma_l(x_0)/\Gamma_0 \neq 1$. The retardation time associated with the dynamics of the Kondo cloud $\tau_\beta = \frac{\hbar\omega_0}{k_B T_K^{min}} \frac{\beta}{2}$ is parametrically large compared to the Kondo cloud formation time [3]. The correction to the quality factor Q_0 of the mechanical system due to retardation effects is determined by the functional form of $f(x) = \frac{\tanh(x)}{\cosh^2(x)} e^{-\frac{\beta}{2}(1+\tanh(x))}$. The time-dependent Kondo temperature in the strong coupling limit at $T \ll T_K^{min}$ is given by

$$k_B T_K(t) = k_B T_K^{min} \exp\left\{\frac{\beta}{2}[1 + \tanh(x(t) - x_0)]\right\}. \quad (5)$$

$k_B T_K^{min}$ plays the role of the cutoff energy for the Kondo problem. As mentioned above, we consider the adiabatically slow motion of the QD, $\hbar\omega_0 \ll k_B T_K^{min}$, provided the condition $\{k_B T, g\mu_B B, eV_{bias}\} \ll k_B T_K^{min}$ is fulfilled.

In order to analyse the amplitude dynamics in the regime of the high-quality resonator $\frac{k_B T_K}{\hbar\omega_0} \ll Q_0$, we apply the Krylov–Bogoliubov averaging method [30]. The amplitude dynamics equations can be obtained by means of the ansatz $x(t) = A(t) \sin(\omega_0 t + \phi)$. In this approximation, we ignore the dynamics of the phase ϕ . The equation for the amplitude dynamics for equation (4) is written as:

$$\dot{A} = -\frac{\gamma}{2}A - \frac{\alpha \tau_\beta}{2\pi}A \int_0^{2\pi} \cos^2 \theta f(A \sin \theta - x_0) d\theta. \quad (6)$$

The results of the numerical analysis of equation (4) are shown in figure 2(a). At zero bias ($\alpha = 0$), equation (4) describes a damped harmonic oscillator with the friction γ . In this case, the

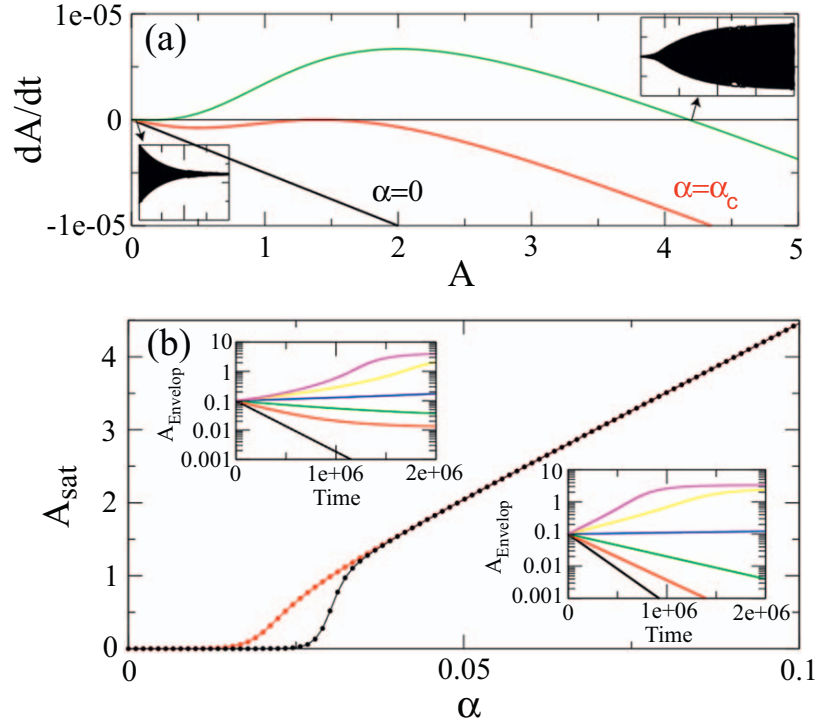


Figure 2. (a) Amplitude dynamics at different values of the dimensionless force α (see details in the text). Insets: the time trace of the oscillation at two different fixed points, indicated by arrows. (b) Saturation amplitude as a function of dimensionless force. The different colors denote the initial conditions near (black dots) and far (red dots) from the equilibrium position x_0 . Insets: the amplitude envelope as a function of dimensionless time calculated using the last (velocity dependent) term in equation (4) responsible for the amplitude dynamics (upper inset) and approximate equation (6) (lower inset). The parameter α varies from $\alpha = 0$ (black) to $\alpha = 0.1$ (magenta). The equations are solved for the following set of parameters: $\beta = 8$, $\gamma = 10^{-5}$, $x_0 = 0.5$ and $\frac{\hbar\omega_0}{k_B T_K^{min}} = 10^{-3}$.

system is characterized by a single stable attracting fixed point at the origin (black line in figure 2(a)).

When the finite bias is applied to the system in the presence of a magnetic field perpendicular to the plane, the increase in the Lorentz force results in the change of the behaviour of the oscillator at some critical value, $\alpha = \alpha_c$. As a result, the equation for the amplitude (equation (6)) acquires an additional non-trivial fixed point for $\dot{A} = 0$, indicated by the red line in figure 2(a). In the regime of $\alpha < \alpha_c$ with a single attracting fixed point at $A = 0$, an assumption $x \approx x_0$ can still be adopted. Under this approximation, equation (6) can be solved analytically. Equation (4) can also be solved by applying the Taylor expansion of hyperbolic functions. Equivalently, the system can be treated as a damped harmonic oscillator with effective friction coefficient $\gamma_{eff} = \gamma \left(1 - \frac{\alpha \tau_p x_0}{\gamma} e^{-\frac{\beta}{2}} \right)$. In the $\alpha \gtrsim \alpha_c$ regime, the system is characterized by two attracting and one repelling fixed points in the space of parameters $\{\alpha, x_0\}$, determined by the equilibrium position of the shuttle, bias and magnetic field as control

parameters. In this regime, the system shows bi-stability and flows either to the fixed point at the origin corresponding to damped oscillations or to the regime of self-sustained oscillation depending on the initial conditions. At $\alpha \gg \alpha_c$, the system falls into the self-sustained oscillations regime.

In figure 2(b), we plot a saturation amplitude of the system as a function of α . The hysteresis of the system is originated from the coexistence of two fixed points characterizing a damped and self-sustained oscillation in the intermediate regime. Moreover, a regime of linearly increasing saturation amplitude exists. Approximating $\tanh x = x$, for $|x| < 1$, and $\tanh x = \text{sign}[x]$ for $|x| > 1$, we rewrite the condition for $\dot{A} = 0$ as

$$\frac{1}{\pi} \int_{-1}^1 \frac{1}{A} \sqrt{1 - \left(\frac{\xi + x_0}{A}\right)^2} \xi (1 - \xi^2) e^{-\frac{\beta}{2}\xi} d\xi = -\frac{\gamma}{\alpha\tau_\beta} e^{\frac{\beta}{2}},$$

where $\xi \equiv A \sin \theta - x_0$. As a result, the saturation amplitude is found as $A_{sat} = \frac{8}{\pi} \frac{1}{\gamma\beta} \frac{\hbar\omega_0}{k_B T_K^{min}} \alpha$, giving rise to the linear slope $(A_{sat} \propto Q_0 \frac{\hbar\omega_0}{k_B T_K^{min}} \frac{\Gamma_0}{E_c})$.

4. Stability and phase diagram

Next, we analyse a stability of the system by linearizing the equations in the vicinity of the stable fixed point describing the stationary states. It is convenient to rewrite equation (4) in the equivalent form of two coupled first-order differential equations:

$$\begin{aligned} \dot{x} &= y \\ \dot{y} &= -x + \frac{\alpha_K(t) + \alpha}{\cosh^2(x - x_0)} - (\alpha\tau_\beta f(x) + \gamma)y \end{aligned} \quad (7)$$

While the position of the fixed point x^* can be found from the condition $x^* \cosh^2(x^* - x_0) = \alpha \left(1 + \delta \exp\left[\frac{\beta}{2}(1 + \tanh(x^* - x_0))\right]\right)$, the corresponding Jacobian matrix is given by

$$J = \begin{pmatrix} 0 & 1 \\ \frac{\alpha g(x^* - x_0)}{\cosh^2(x^* - x_0)} - 1 & -\alpha\tau_\beta f(x^* - x_0) - \gamma \end{pmatrix},$$

where $g(x) = \delta \left(\frac{\beta}{2 \cosh(x)} - 2 \tanh(x)\right) \exp\left[\frac{\beta}{2}(1 + \tanh(x))\right] - 2 \tanh(x)$ and δ is the ratio between the α and Kondo force at the minimal Kondo temperature. Interestingly, this condition allows a regime of multiple solutions for x^* depending on $|x_0|$ and α . In figure 3(a), we plot the stability diagram of the Jacobian matrix in the parameter space $\{\alpha, x_0\}$. The linearized system can be categorized by a stable focus, unstable focus, and a saddle point.

First, we consider a single-solution regime for the fixed point x^* . In this case, instability arises in the absence of a stable focus (a negative quality factor characterizing an increment of the oscillations). The negative Q corresponds to the pumping regime, where the system is effectively ‘heated’ in contrast to the damping regime of $Q > 0$, which may be interpreted as effective cooling of a shuttling device. The positive values of $\text{Re}(\lambda_\pm)$ give rise to the regime of

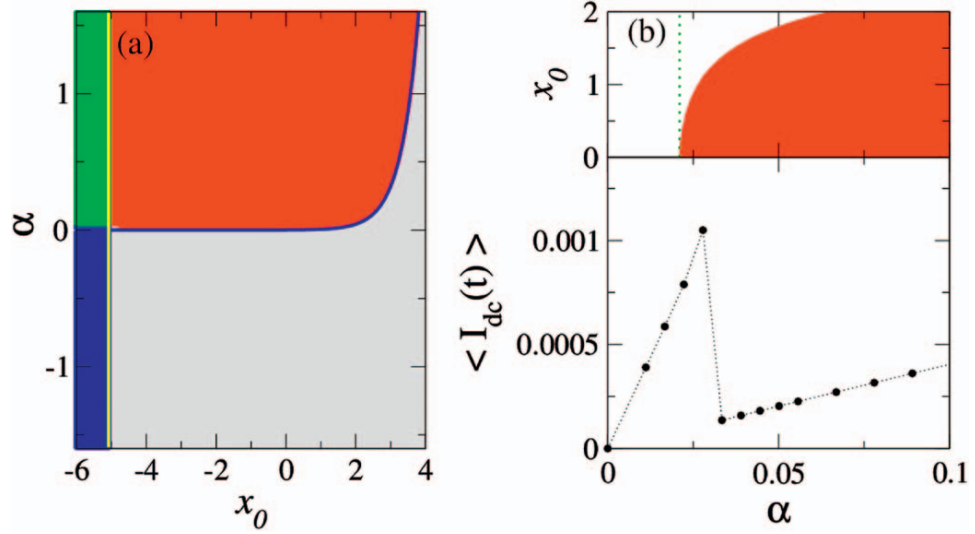


Figure 3. (a) Stability diagram in the phase space of asymmetry parameter x_0 and dimensionless force α . The different colors correspond to different classes of stability: stable focus (gray regime), unstable focus (red and green regimes, depending on initial conditions), and saddle point (green and blue regimes, see text for details). The weak out of equilibrium condition used in the calculations is determined by $-\frac{eV_{bias}}{k_B T_K^{min}} \cdot \frac{g\mu_B B}{k_B T_K^{min}} \leq 0.1$, and $\alpha \cdot \delta = 50.27$. The blue solid lines are drawn in accordance with equation (8), and the yellow solid line determines the boundaries of a multi-valued solution. (b) The upper panel is a fragment of phase diagram (a), and the green dotted line represents a condition $\alpha = \gamma/\tau_\beta |f(x_{un})|$ determined by the eigenvalues of the Jacobian matrix. The lower panel shows the average current $\langle I_{dc} \rangle$ as a function of α at $x_0 = 1.0$. It is seen that the transition from unstable focus to stable focus can be realized by changing the direction of magnetic field $B \rightarrow -B$ at given V_{bias} .

instability when both $\alpha > 0$ and $\alpha > \frac{\gamma}{\tau_\beta |f(x_{un})|}$ are satisfied. The critical values for the instability are given by a functional shape of $f(x)$ with $\alpha = \gamma/\tau_\beta |f(x_{un})|$, (green dotted line in figure 3(b)), where $x_{un} \cong x_0 + \tanh^{-1}\left(\frac{3 - \sqrt{9 + \beta(\beta + 2)}}{\beta}\right) \approx x_0 + \tanh^{-1}(-1 + 2/\beta)$. Thus, the critical values of α for the unstable regime depend on the quality factor, which is given by, $\alpha_+^{un} \gtrsim k_B T_K / \hbar \omega_0 \cdot 1/Q_0$. Second, the regime of the multi-valued solution is determined by $1 < \frac{\alpha g(x^* - x_0)}{\cosh^2(x^* - x_0)}$ (yellow solid line in figure 3(a)). The saddle point solution leads to a bi-stability of the system under certain conditions for the Q factor.

The approximate solution determining the boundaries for the instability regime of the applied magnetic field is given by:

$$\frac{\gamma}{4\tau_\beta} \exp\left[-\frac{\beta}{2} + 2x_0\right] < \alpha, \quad (8)$$

This condition is valid for the range of magnetic fields; $\frac{m\omega_0^2 \lambda \phi_0 k_B T_K}{eV_{bias} L \hbar \omega_0 Q_0} < B$. The upper limit of this domain of validity is determined by the smallest value of two contributions, namely the emf

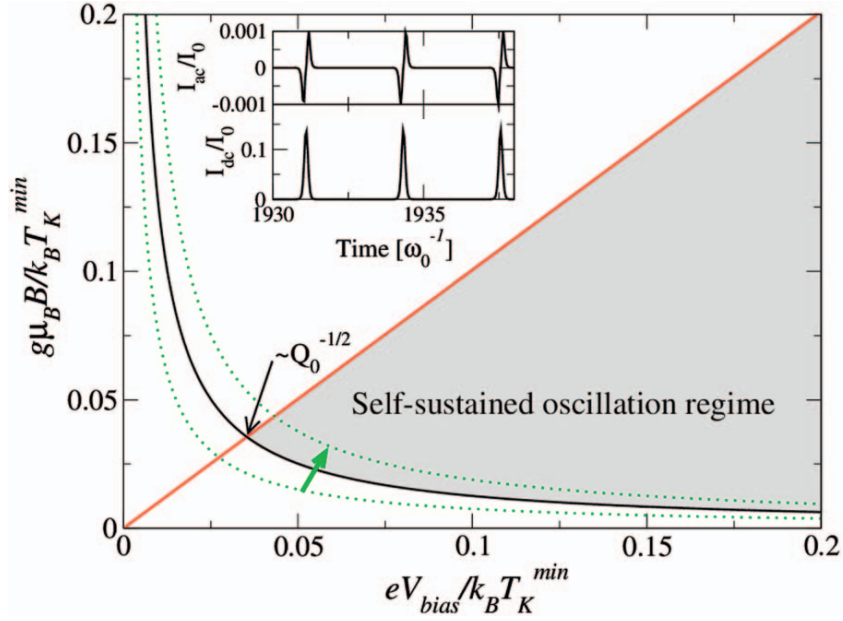


Figure 4. Stability (phase) diagram in a parameter space of $\frac{g\mu_B B}{k_B T_K^{\min}}$, and $\frac{eV_{\text{bias}}}{k_B T_K}$. The calculations are performed at $\beta = 8$, $\frac{\hbar\omega_0}{k_B T_K^{\min}} = 10^{-3}$, $\alpha \cdot \delta = 50.25$. The red line is defined by the condition $B < \frac{E_x eV_{\text{bias}} \lambda \phi_0}{\Gamma_0 k_B T_K^{\min} L \lambda^2}$. The α parameter increases for the transition from the lower to upper green dotted line (see details in the text). The green arrow shows how one enters the self-sustained oscillation regime by changing the force at a given anisotropy parameter. Inset: time trace of the tunnel current contribution in the steady-state regime under the parameters of $x_0 = 0.5$, $\frac{eV_{\text{bias}}}{k_B T_K^{\min}} = 0.1$, $\frac{g\mu_B B}{k_B T_K^{\min}} = 0.1$, and $I_0 = \frac{m\omega_0^2 \lambda}{BL}$.

force and the asymmetry condition. Taking into account all necessary constraints for the stability regimes, we construct the phase diagram of our model (see figure 4). This phase diagram shows the boundaries for the self-sustained oscillations regime (gray). Two green dotted lines correspond to two different values of parameter α , while the green arrow moves in a direction of increasing α . The red line is defined by the condition $B < \frac{E_x eV_{\text{bias}} \lambda \phi_0}{\Gamma_0 k_B T_K^{\min} L \lambda^2}$ (see [3]), and the black line is determined by the critical value of asymmetry parameter x_c as a function of the Q -factor and Kondo temperature T_K^{\min} : $x_c = \frac{k_B T_K^{\min}}{\hbar\omega_0} \frac{1}{Q_0}$. Thus, the upper limit of the instability regime under the condition of fixed asymmetry parameter $x_c < x_0$ is described by $B/B_0 < \frac{E_c eV_{\text{bias}}}{\Gamma_0 k_B T_K^{\min}}$, where B_0 is the magnetic field corresponding to the flux quanta through the $\lambda \cdot L$ square. The periodic splashes of I_{dc} and I_{ac} near the turning points of the shuttle [3] are shown in the lower and upper insets, respectively. The change in average dc current $\langle I_{dc}(t) \rangle$ in transition from the damping oscillations regime to the self-sustained oscillation regime with increasing α is illustrated in figure 3(b).

Plugging in some typical values of m , λ , ω_0 and Q_0 into the conditions for the upper and lower bounds of the instability regime: $m = 10^{-19} - 10^{-21}$ kg, $\lambda = 1\text{\AA}$, and $\omega_0 = 10^7 - 10^9$ Hz,

$Q_0 = 10^5 - 10^7$ allows one to estimate the range of magnetic fields and bias voltages for the self-sustained oscillations in the Kondo shuttling regime: $1 T < B < 10 T$, $\frac{eV_{bias}}{k_B T_K} = 0.1$, $\frac{\hbar\omega_0}{k_B T_K^{min}} = 10^{-3}$. This range of parameters covers cantilever materials from light single-walled carbon nanotubes to relatively heavy SiN. The range of quality factors refers to the best known nano-mechanical devices [31].

5. Summary

Summarizing, we analysed a fully fledged stability diagram of the Kondo shuttle device, subject to both variation in the external dc electric and magnetic fields, and asymmetry of the tunnel barriers. The Kondo effect, with its anomalously long relaxation dynamical spin screening time, is an ideal tool for coupling spin and mechanical degrees of freedom. We have shown that the competition between the mechanical damping of the oscillator at zero field, zero bias and the contribution coming from the strong resonance spin scattering (Kondo effect) results in the loss of mechanical stability, manifested in two different regimes of NEM/NSM oscillations. Namely, if the Kondo force controlled by external fields further damps the oscillator, we obtain an efficient mechanism of cooling the nano-shuttle. On the other hand, if the contribution of the Kondo force enhances the oscillations, we arrive at the non-linear steady-state regime of self-sustained oscillations. We found the critical values of the external fields and asymmetry parameter determining the instability regimes for adiabatic Kondo shuttling. The phase diagram of the Kondo shuttle model is constructed by taking into account the limitations given by the electromotive force, which always contributes to the friction. We have shown that due to the exponential sensitivity of the Kondo effect to external parameters, and the strong coupling between the mechanical and electron (spin) degrees of freedom, the device including an element with localized spin acquires super-high tunability. We suggested an experimental setup to realize the Kondo shuttling instability and estimated all the necessary conditions for this. We believe that experiments with such a setup can provide valuable information on the kinetics of the formation of the Kondo cloud, and eventually the Kondo shuttle can be used for experimental spin manipulation in nano-spintronic devices.

Acknowledgments

We appreciate illuminating discussions with B L Altshuler, Ya Blanter, S Flach, F Marquardt, N Prokof'ev and E Weig. The research of MNK was supported in part by the National Science Foundation under Grant No. NSF PHY11-25915. The research of KK was partially supported by ISF Grant No. 400/12, and the work of RIS and LYG was supported in part by the Swedish VR.

References

- [1] Shekhter R I, Gorelik L Y, Krive I V, Kiselev M N, Parafilo A V and Jonson M 2013 Nanoelectromechanics of shuttle devices *Nanoelectromech. Syst.* **1** 1–25
- [2] Kiselev M N, Kikoin K, Shekhter R I and Vinokur V M 2006 Kondo shuttling in a nanoelectromechanical single-electron transistor *Phys. Rev. B* **74** 233403

- [3] Kiselev M N, Kikoin K A, Gorelik L Y and Shekhter R I 2013 Kondo force in shuttling devices: dynamical probe for a Kondo cloud *Phys. Rev. Lett.* **110** 066804
- [4] Kondo J 1964 Resistance minimum in dilute magnetic alloys *Prog. Theor. Phys.* **32** 37
- [5] Pustilnik M and Glazman L 2004 Kondo effect in quantum dots *J. Phys.: Condens. Matter* **16** R513
- [6] Borda L 2007 Kondo screening cloud in a one-dimensional wire: numerical renormalization group study *Phys. Rev. B* **75** 041307(R)
- [7] Park J, Lee S-S B, Oreg Y and Sim H S 2013 How to directly measure a Kondo clouds length *Phys. Rev. Lett.* **110** 246603
- [8] Gubernatis J E, Hirsch J E and Scalapino D J 1987 Spin and charge correlations around an Anderson magnetic impurity *Phys. Rev. B* **35** 8478
- [9] Holzner A, McCulloch I P, Schollwöck U, Delft J and Heidrich-Meisner F 2009 Kondo screening cloud in the single-impurity Anderson model: a density matrix renormalization group study *Phys. Rev. B* **80** 205114
- [10] Affleck I and Simon P 2001 Detecting the Kondo screening cloud around a quantum dot *Phys. Rev. Lett.* **86** 2854
- [11] Affleck I 2009 *Perspectives of Mesoscopic Physics—Dedicated to Prof. Yoseph Imry's 70th Birthday* (World Scientific)
- [12] Mitchell A K, Becker M and Bulla R 2011 Real-space renormalization group flow in quantum impurity systems: Local moment formation and the Kondo screening cloud *Phys. Rev. B* **84** 115120
- [13] Bösser C A, Martins G B, Costa Ribeiro L, Vernek E, Anda E V and Dagotto E 2010 Numerical analysis of the spatial range of the Kondo effective *Phys. Rev. B* **81** 045111
- [14] Boyce J P and Slichter C P 1974 Conduction-electron spin density around Fe impurities in Cu above and below T_K *Phys. Rev. Lett.* **32** 61
- [15] Kinaret J M, Nord T and Viefers S 2003 A carbon-nanotube-based nanorelay *Appl. Phys. Lett.* **82** 1287
- [16] Bennett S D, Cockins L, Miyahara Y, Grutter P and Clerk 2010 A strong electromechanical coupling of an atomic force microscope cantilever to a quantum dot *Phys. Rev. Lett.* **104** 017203
- [17] Cockins L, Miyahara Y, Bennett S D, Clerk A, Studenikin S, Poole P, Sachrajda A and Grutter P 2010 Energy levels of few-electron quantum dots imaged and characterized by atomic force microscopy *Proc. Natl. Acad. Sci. USA* **107** 9496
- [18] Azuma Y, Hatanaka T, Kanehara M, Teranishi T, Chorley S, Prance J, Smith C G and Majima Y 2007 One by one single-electron transport in nanomechanical Coulomb blockade shuttle *Appl. Phys. Lett.* **91** 053120
- [19] Gorelik L Y, Isacsson A, Voinova M V, Kasemo B, Shekhter R I and Jonson M 1998 Shuttle mechanism for charge transfer in Coulomb blockade nanostructures *Phys. Rev. Lett.* **80** 4526
- [20] Fedorets D, Gorelik L Y, Shekhter R I and Jonson M 2004 Quantum shuttle phenomena in a nanoelectromechanical single-electron transistor *Phys. Rev. Lett.* **92** 166801
- [21] Shekhter R I, Santandrea F, Sonne G, Gorelik L Y and Jonson M 2009 Nonequilibrium and quantum coherent phenomena in the electromechanics of suspended nanowires *Low Temp. Phys.* **35** 662
- [22] Shekhter R I, Gorelik L Y, Glazman L I and Jonson M 2006 Electronic Aharonov–Bohm effect induced by quantum vibrations *Phys. Rev. Lett.* **97** 156801
- [23] Radic D, Nordenfelt A, Kadigrobov A M, Shekhter R I, Jonson M and Gorelik L Y 2011 Spin-controlled nanomechanics induced by single-electron tunneling *Phys. Rev. Lett.* **107** 236802
- [24] Cohen G, Fleurov V and Kikoin K 2009 Time-dependent single electron tunneling through a shuttling nanoisland *Phys. Rev. B* **79** 245307
- [25] Nordenfeld A, Tarakanov Y, Gorelik L Y, Shekhter R I and Jonson M 2010 Magnetomotive instability and generation of mechanical vibrations in suspended semiconducting carbon nanotubes *New J. Phys.* **12** 123013
- [26] Hüttel A K, Witkamp B, Leijnse M, Wegewijs M R and van der Zant H S J 2009 Pumping of vibrational excitations in the Coulomb-blockade regime in a suspended carbon nanotube *Phys. Rev. Lett.* **102** 225501
- [27] Faust T, Krenn P, Manus S, Kotthaus J P and Weig E M 2012 Microwave cavity-enhanced transduction for plug and play nanomechanics at room temperature *Nat. Commun.* **3** 728

- [28] Hewson A 1997 *The Kondo Problem to Heavy Fermions* 2nd edn (Cambridge: Cambridge University Press)
- [29] Andrei N, Furuya K and Lowenstein J H 1983 Solution of the Kondo problem *Rev. Mod. Phys.* **55** 331
- [30] Vidyasagar M 1993 *Nonlinear Systems Analysis* (Chichester: Prentice-Hall)
- [31] Faust T, Rieger J, Seitner M J, Kotthaus J P and Weig E M 2013 arXiv:[1310.3671](https://arxiv.org/abs/1310.3671)